Tracking Aggregation and Fibrillation of Globular Proteins Using Terahertz and Far-Infrared Spectroscopies

Gretel M. Png, *Member, IEEE*, Robert J. Falconer, and Derek Abbott, *Fellow, IEEE*

***Abstract*—Partially unfolded proteins can self-assemble to form insoluble protein fibrils with diameters in the nanometer scale. These are of particular interest in healthcare because of their presence in diseases such as Alzheimer's disease and type-II diabetes. Tracking the formation of protein fibrils has far-reaching benefits for research into treatment of these diseases. Current optical techniques that track fibrillation either limit samples to their aqueous form or are slow to conduct. We present in this work terahertz and far-infrared (FIR) spectroscopic analyses of fibrils made from three globular proteins. We track the fibrillation process over an extended period to show that mature fibrils have distinct absorbance properties that are not solely caused by scattering. Results also show that FIR spectroscopy can provide information about fibril structures that is otherwise missed by optical techniques.**

***Index Terms*—Amyloid fibrils, far-infrared (FIR), protein aggregation, spectroscopy, terahertz (THz).**

I. Introduction

PROTEIN aggregation is the process in which protein molecules accumulate to form either disordered or ordered microstructures. While disordered protein microstructures do not have a fixed three-dimensional (3-D) structure, ordered protein microstructures have shapes that include fibrils, spheres, amorphous clumps, and gels [1]–[3].

Fibrillar protein microstructures are of particular interest because they are present in a class of diseases called *amyloidoses*, which includes Alzheimer's disease and type-II diabetes. Extracellular accumulation of these fibrillar microstructures called amyloid fibrils is believed to cause degeneration of tissues and organs. Fibrillar protein microstructures are also of interest in nonpathogenic applications. Protein fibrils have been used to create the base upon which drug-delivery gels can be synthesized [4]. In the food industry, protein fibrils have the potential to modify food texture as well as improve manufacturing processes [5]. The study of protein fibrils is therefore useful to a wide range of real-world applications.

Many ordered biomolecules have phonon resonances in the terahertz (THz) and far-infrared (FIR) spectral regions. For example, the ordered crystalline structures of saccharides (e.g., α-lactose) produce a wealth of resonances that are well documented in literature [6]–[8]. Ordered protein crystals have also been reported to produce phonon resonances in the THz and FIR range [9], [10].

Ordered protein fibrils were expected to also produce rich resonances in the THz and FIR ranges but none have been observed for fibrils synthesized from lysozyme and insulin [11], [12]. Lyophilized lysozyme fibrils are reported in [11] to show little differentiation from lysozyme monomers (a molecular unit of lysozyme) in the low THz frequency range. At higher frequencies, however, the fibrils scatter FIR radiation more strongly than lysozyme monomers and the scattering nature of the fibrils is deemed a limitation to the usefulness of THz/FIR spectroscopy in studying fibrils. We show in this paper that scattering is not the sole contributor to the measured signal and that THz/FIR spectroscopy can be useful for tracking fibrillation. The fibrillation process is dynamic, and there are hypotheses that fibrils in intermediate stages of fibrillation can also be pathogens in amyloidosis [13]–[15]. Similarly, in food technology, proteins in different stages of fibrillation have immense impact on food texture and processibility [16]–[18], thus it is useful to develop strategies for tracking protein fibrillation.

Optical techniques such as fluorescence, circular dichroism, and light scattering do currently exist for examining protein fibrils, but these techniques require samples to be suspended in optically clear solvents [19]. Terahertz and FIR spectroscopies have the advantage of not requiring optical clarity but rather spectroscopic transparency of the solvent in the THz/FIR frequency range. Transmission electron microscopy (TEM) allow visual verification of fibrils but the sample preparation and subsequent inspection with the electron microscope is a slow process. Terahertz and FIR spectroscopies are comparatively faster than TEM inspection.

This paper presents an analysis of lysozyme, insulin and BSA fibrils measured directly (nonlyophilized) with a THz time-domain spectroscopic system (THz-TDS) and a synchrotron FIR light source. We demonstrate that FIR spectroscopy can be used to track the fibrillation process of these proteins as they aggregate from native globular protein to highly dense fibrillar compositions. We extend the incubation time of the fibrils be-

Manuscript received August 14, 2015; revised November 12, 2015; accepted November 29, 2015. Date of publication December 24, 2015; date of current version January 20, 2016. The work of G. M. Png was supported by the Australian Research Council through Grant DE120101494. The work of D. Abbot was supported by the Australian Research Council Future Fellowship under Grant FT100100585.

G. M. Png and D. Abbott are with the School of Electrical and Electronic Engineering, University of Adelaide, South Australia 5005, Australia (e-mail: gretel.png@adelaide.edu.au).

R. J. Falconer is with the Department of Chemical and Biological Engineering, ChELSI Institute, University of Sheffield, Sheffield S1 3JD, U.K.

Color versions of one or more of the figures in this paper are available online at http://ieeexplore.ieee.org.

Digital Object Identifier 10.1109/TTHZ.2015.2505900

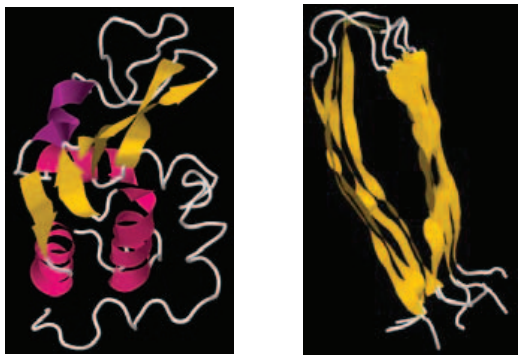

(a) (b)

Fig. 1. (a) Native lysozyme molecule contains α-helices (red), random coils (white), and β-sheets (yellow). (b) Fibrils predominantly contain β-sheets. Images rendered with Jmol (PDB ID: 2LYZ and 2NNT, respectively).

yond those reported previously, leading to significant spectral changes not observed before. Complementary findings using circular dichroism, fluorescence, and electron microscopy aid in correlating the structural changes with the spectral changes.

The organization of this paper is as follows. First, we briefly discuss the biophysical changes that occur in protein aggregation, with emphasis on fibril formation. Materials and methods used in this study are then introduced. THz time-domain spectroscopy (TDS) and synchrotron-based FIR results are then presented and discussed.

II. Biophysical Changes in Protein Aggregation

There are many pathways for protein aggregation [1], but we will focus on the factors that trigger fibril formation. Heat can lead to partial unfolding of the protein structure, which under acidic conditions can lead to the proteins self-assembling.

When a protein molecule such as that shown in Fig. 1(a) is heated in an aqueous environment, it unfolds and exposes parts of its structure (amino acid residues) that are hydrophobic. A hydrophobic residue quickly seeks to form intermolecular interactions with another hydrophobic residue from a different molecule. Dimers, tetramers, and eventually large insoluble oligomers are formed [2].

Fibril formation differs from amorphous aggregation in that a secondary structure called β-pleated sheets as shown in Fig. 1(b) can form between the neighboring proteins, providing a template for the further formation of β-pleated sheets. The β-pleated sheets, which can be visualized as a corrugated sheet with parallel undulations, dominate the structure of the oligomers, resulting in their fibrillar appearance. The fibrillar oligomers may then proceed to coil together to form thicker fibrils as aggregation progresses [20], [21]. Fibrils at different stages of aggregation are studied in this work and the results will be presented in Sections V and VI.

III. Materials

There are many recipes reported in existing literature for synthesizing fibrils but we follow the ones in [11] and [12] so that we can compare our findings fairly for lysozyme and insulin. For BSA, we follow the recipe in [21].

A. Synthesizing Lysozyme Fibrils

Native lysozyme (Sigma-Aldrich L6876) is dissolved at a concentration of 20 mg/ml in a pH 2 buffer containing 200 ppm sodium azide for retarding bacterial growth. The buffer consists of glacial acetic acid in MilliQ water. To remove salt particles that are present in commercial lysozyme, the lysozyme solution is dialyzed in buffer for 3 h using Cellusep T2 dialysis membranes. As per the manufacturer instructions, low-molecular-weight salts usually equilibrate within 3 h and two rounds of dialysis with fresh buffer are usually sufficient. The lysozyme solution is then filtered with Millipore 0.22-μm syringe filters before being distributed into aliquots. One aliquot is immediately refrigerated at 4 °C—this is the negative control. The remaining aliquots are incubated without agitation in a water bath at 57 °C. Aliquots are removed from the water bath at 24-h intervals starting at 24 h from the start of incubation up to 144 h.

B. Synthesizing Insulin Fibrils

Native insulin (Sigma-Aldrich I6634) is dissolved at a concentration of 2 mg/ml in a pH 2 buffer containing glacial acetic acid in MilliQ water. We modify the recipe in [12] because the 20% acetic acid solution reported was found to be too acidic, possibly due to our use of glacial acetic acid; the resultant concentration of the acetic acid solution is 12%. The insulin solution is distributed into aliquots after the insulin is dissolved using a platform shaker. One aliquot is immediately refrigerated at 4 °C to be the negative control. The remaining aliquots are incubated without agitation in a water bath at 60 °C. Aliquots are removed from the water bath at the same intervals as mentioned in Section III-A.

C. Synthesizing BSA Fibrils

Native BSA (Sigma-Aldrich A7906) is dissolved at a concentration of 2 mg/ml in a pH 7.4, 20 mM Tris-HCl buffer made from stocks of 0.2-M Tris solution and 0.2-M HCl solution. The BSA solution is then filtered with Millipore 0.22-μm syringe filters before being distributed into aliquots. One aliquot is immediately refrigerated at 4 °C to be the negative control. The remaining aliquots are incubated without agitation in a water bath at 67.5 °C. Aliquots are removed from the water bath at the same intervals as mentioned in Section III-A.

IV. Equipment and Methods

Three optical techniques are routinely used to verify the structure and presence of fibrils: transmission electron microscopy (TEM) to verify large-scale structure (tens of nanometers), circular dichroism to verify secondary structure (tenth of a nanometer) and fluorescence spectrometry to verify formation of amyloid fibrils [22]. These techniques will be briefly described in the following subsections together with relevant results from this study. We also introduce the THz and FIR equipment used as well as the sample holding technique employed in this work.

A. Transmission Electron Microscopy

TEM allows for visual inspection of the samples. We utilize a Tecnai Spirit TEM with 100-kV accelerating voltage. Samples are mounted on the Formvar support film of 200-mesh carbon-

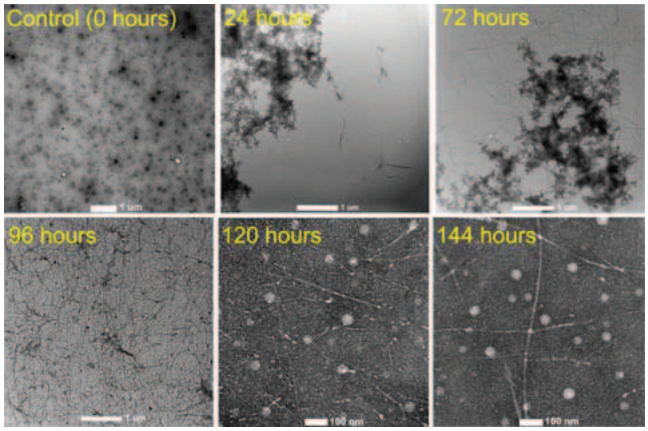

Fig. 2. TEM micrographs of insulin fibrils showing the progress of fibrillation. (a) The control sample only contains globular insulin proteins hence no fibrils are visible. (b) The proteins aggregate to form thick clumps shortly after incubation begins. After 24 h, some fibrils are evident. (c) Fibrillation intensifies as fibrils increase in number and length, but the protein clumps still exist. (d) A dense network of fine fibrils is present. (e) Individual fibrils thicken. (f) Individual fibrils further thicken and lengthen. Scale bar representation: 1 μm for 0–96 h; 100 nm for 120 and 144 h.

coated copper grids (Proscitech GSCU200CH-100). The acidic lysozyme and insulin samples are diluted 10:1 to prevent breakage of the Formvar film. Uranyl acetate is applied to negatively stain the grids.

Fig. 2 shows a representation of fibrils formed over time. The actual appearances of the fibrils and the rate of fibrillation differ for the three protein samples used in this work. However fibrillation progresses on a similar path thus only the images of insulin fibrils are presented here. Clumps formed at the start of incubation undergo fibrillation to become fibrils. The mature fibrils are thick and long and form a dense network that appears cloudy when visually inspected.

B. Circular Dichroism

Circular dichroism (CD) is a spectroscopic technique that identifies the dominant secondary structure of a protein molecule, i.e., α-helices, random coils or β-sheets, by measuring the difference in far-ultraviolet absorption between right- and left-circularly polarized light as the two light orientations pass through a sample. More information about CD can be found in [23].

We use the Jasco J-815 CD spectrometer and a quartz cuvette with 1-mm pathlength. To avoid saturating the spectrometer, it is necessary to dilute some of the samples with dilution ratios as noted in Fig. 3. The buffer does not contain any protein thus has no absorption difference. The control sample and the 24-h-old sample contain mainly α-helices [Fig. 1(a)], which are identified by the troughs at 208 nm and 222 nm. As β-sheets form, the CD profile becomes a lopsided parabola with less intense optical ellipticity as seen for the 72-, 120- and 144-h-old samples. This observation is common across all proteins used in this work hence only the CD profiles of BSA are presented here.

C. Fluorescence Spectrometric Assay

Fluorescence spectrometric assay utilizes a dye to identify the presence of amyloid fibrils in a protein sample. The Thioflavin-T (ThT, Sigma-Aldrich T3516) dye binds to the

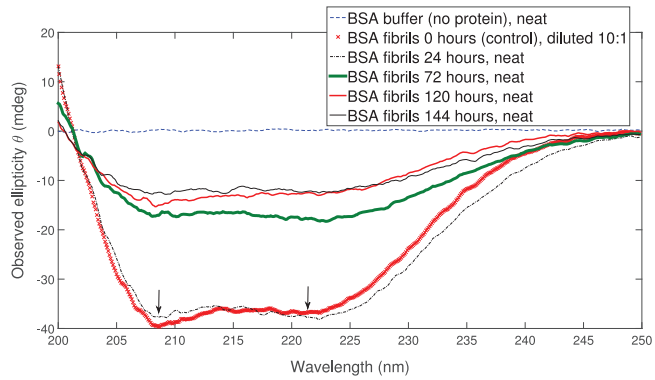

Fig. 3. Circular dichroism spectral profiles of one of the BSA samples. Circular dichroism is used to verify the presence of β-sheets. Dilution is necessary to keep the photomultiplier tube voltage ('HT voltage') below 600 V. Two distinct troughs, as indicated by the arrows, at 208 nm and 222 nm for the control sample and the 24-h-old sample confirm their predominant α-helical structure. The spectra of the older samples are more lopsided parabolic, confirming the depletion of α-helical structure during fibril formation. In the above legend, 'neat' indicates an undiluted solution.

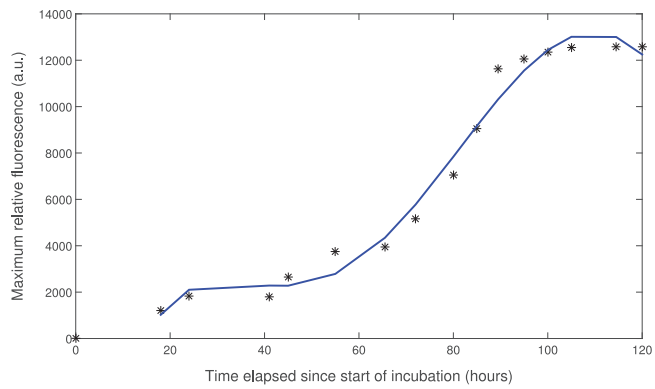

Fig. 4. Outcome of a ThT fluorescence assay on lysozyme. The S-shaped plot confirms the usual progress of fibrillation that begins slowly but then rises quickly before reaching a plateau. The blue solid line is a line fit of the data obtained at different points in time during the 120 h of incubation.

long axis in amyloid fibrils and exhibits strong fluorescence between 465–565 nm when excited with light at a wavelength of ≈450 nm [24]. We utilize a Fluostar Optima (BMG Labtech) 96-well plate reader with 425-nm laser emission and 490-nm fluorescence detection. In each well of the plate, 20 μl of 20-μM ThT solution is added to 180 μl of test sample.

The S-shaped profile in Fig. 4 confirms amyloid fibrillation, showing the weak fluorescence at the early stage of incubation followed by a sharp rise in fluorescence as fibrillation occurs, finally plateauing when fibrillation slows down with few vacant binding sites left on the amyloid fibrils.

D. Terahertz Time-Domain Spectroscopy (THz-TDS)

For experiments conducted in the lower THz frequency range ($\leq$2 THz), we utilize a Menlo Tera K15 modular THz-TDS system. In summary, this system contains a femtosecond laser source that is fiber-coupled to an optical light path with a delay line and to the THz emitter and detector modules. A stripline photoconductive antenna (PCA) is used for THz emission, and a PCA antenna is used for detection. Each recorded data set is

averaged over three scans. Each plot presented in this paper is averaged over three recorded data sets (i.e., nine scans).

Measurements are made, with nitrogen purging, both at room temperature (293 K) and with cryogenic cooling down to 123 K. A helium-cooled, closed-cycle cryostat (Janis CCS-450) is used to achieve the cryogenic temperature. The sample holder of the cryostat extends into the path of the THz-TDS system thus is included in the nitrogen-purged environment. The cryogenic temperature of 123 K is chosen because our previous study of protein gels at cryogenic temperatures showed no significant difference in the measured signal at 123 K and at 20 K [25].

E. Fourier Transform Infra-Red (FTIR)

For experiments conducted in the higher THz frequency range (>2 to 18 THz), we utilize a Fourier transform infrared (FTIR) spectrometer (Bruker IFS 125/HR) with a synchrotron radiation source (Australian Synchrotron, Clayton, Victoria) in conjunction with a 6-μm multilayer mylar beamsplitter. Measurements are made at 77 K under vacuum using a liquid nitrogen-cooled cryostat (Janis VPF-100-FTIR). Signals are detected with a liquid helium-cooled Si bolometer. Each recorded data set is averaged over 100 scans; we record five data sets per sample.

F. Sample Holding Technique

We utilize the nitrocellulose (NC) membrane-based sample holding technique previously reported in [26], where we have reported that the THz and FIR optical properties of the NC membranes lie between those of high-density polyethylene (HDPE) and ultra-high molecular weight polyethylene. Additionally, we are able to directly apply aqueous samples on the NC membranes without the need for an extra bulking medium.

In summary, 600 μl of aqueous sample is distributed across two NC membranes and allowed to air-dry extensively in a vacuum-pumped desiccator. This sample volume is used because it is the liquid holding limit of the NC membrane. When the membranes appear visually to be dry, the two membranes are combined so that the sample is sandwiched between the membranes and can then be placed in the path of the THz radiation. Due to the small sample volume involved, it is not possible to accurately measure the sample thickness as described in [26], thus we will report our findings in this paper in terms of relative absorbance (with respect to NC) with arbitrary units.

V. THz-TDS Results and Discussion

To ascertain if air-drying of the protein fibrils has sufficiently removed all moisture from the samples, we track the THz absorbance of BSA fibrils over a span of ≈50 min. Fibrillation in BSA produces thick clumps of fibrils that will trap most moisture thus BSA fibrils are best candidates for this task. Fig. 5 shows that the sample continues to dry out, eventually reaching a quasi-steady state upon which little or no further change to the absorbance is apparent. This is the state on which we base our observations in this work for the three protein fibrils studied.

The THz absorbance of the buffer as shown in Fig. 5 is zero as expected since there is no protein in the buffer; it is expected

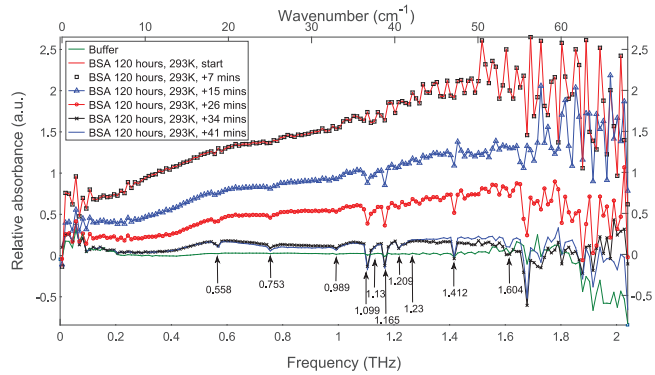

Fig. 5. Tracking dehydration of 600 μl of BSA fibrils held in NC, measured in a nitrogen-purged chamber. Multiple measurements made over time show the sample continues to dry in the sample chamber, eventually reaching a non-zero absorbance steady state where no further changes to the absorbance is observed. Unlike the BSA fibrils, the buffer has near zero absorbance when at a steady state. Positions of known water vapor lines as reported in [27], [28] are as indicated by the arrows.

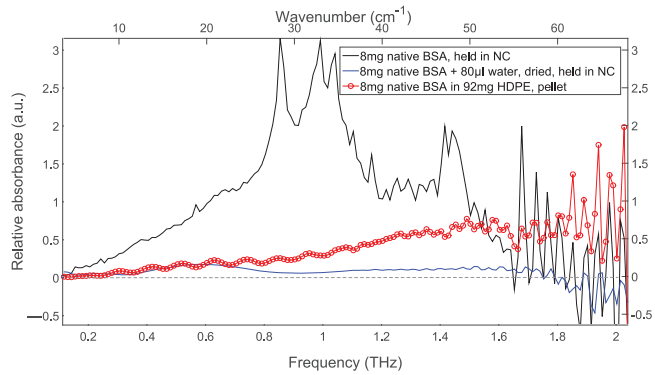

Fig. 6. Comparison of the relative absorbance of dry and hydrated native BSA, held in NC and pressed as a pellet. When compared with the pellet, NC-held native BSA scatters THz radiation more strongly as shown by the steep rise in absorbance (the peaks are due to the measured signal exceeding the maximum detectable THz absorbance). The hydrated native BSA has reached the steady dehydrated state as described in Fig. 5, but its absorbance property at this state does not resemble that of native BSA in NC, indicating the continued presence of water.

to behave like water and dehydrate completely. The THz absorbance of BSA fibril is dissimilar to that of the buffer, which is encouraging as this means that our THz-TDS system and NC-holding technique are sensitive enough to differentiate between buffer and fibrils. However the magnitude of the fibrils' absorbance hovers above zero up to ≈1.5 THz, with a distinct hump at 0.6 THz; we had expected a linearly rising THz absorbance profile as reported in [11].

The spectral profile observed in our work may be due to the presence of residual water that is keeping the fibrils in a hydrated state, or due to the low concentration of protein present in 600 μl of aqueous sample (1.2 mg for BSA and insulin, 12 mg for lysozyme). To answer both questions, we measure 8 mg of dry and wet native BSA in the NC holder. Additionally, we also measure 8 mg of native BSA pressed with HDPE into a pellet; Fig. 6 presents a comparison of their THz absorbance. As expected, without the presence of a bulking medium such as HDPE, the NC-held native BSA strongly scatters the THz radiation due to the large size of the BSA crystals.

The hydrated native BSA sample has more than six times the protein concentration of that in BSA fibrils thus it is expected that upon drying, the THz absorbance will be similar to that of dry native BSA. This expectation is based on previous observations of hydrated α-lactose whereby the THz absorbance after drying was similar to that of native α-lactose [26], [29]. As shown in Fig. 6 however, the THz absorbance of the dehydrated (air-dried) native BSA does not resemble that of dry native BSA. The difference between the two THz absorbance profiles indicates that some residual water is still present in the dehydrated sample.

Bound water, which is water that is bound to a protein molecule, was reported as being the last water to be removed from a sample undergoing lyophilization [30]. We therefore hypothesize that our air-dried samples still contain bound water and very possibly also contain free water inside and outside the protein's hydration shell, whereby these water molecules cannot be removed by simple air-drying. The ramification of the above observation is that at room temperature, the fibrils measured in our work still contain water to preserve the fibrils in their hydrated state but that the water content, unlike bulk liquid water, is insufficient to strongly attenuate the transmitted THz radiation.

Fig. 7 presents the THz absorbance profiles of our fibrils and their control samples at room temperature. Lysozyme, BSA and insulin are all globular proteins in their native form thus the control samples at 0 hours are expected to contain mostly globular proteins, however there is little differentiation between the lysozyme and insulin fibrils and their control samples.

The BSA fibrils are distinct from their control sample but as mentioned at the start of this section, BSA forms thick clumps of fibrils that trap moisture hence it is expected that the stronger THz absorbance is due to the higher water content in BSA fibrils rather than due to the fibrils. This is confirmed at cryogenic temperatures at which the residual water is frozen so as not to interfere with the measured signal. Attenuation by the polyethylene windows used in our cryostat has restricted the spectral bandwidth to $\approx$0.8 THz and has introduced substantial noise to the measured signals hence we do not show the results. Nonetheless, the limited data available indicates that the BSA fibrils and control sample have similar THz absorbance up to $\approx$0.5 THz. From 0.5 to 0.8 THz, there appears to be a slight increase in the THz absorbance of the fibrils; this is also observed for insulin. For lysozyme, the difference appears to be constant up to 0.8 THz. While these outcomes support the argument that THz-TDS can be used to track aggregation, the limited bandwidth and high noise level are of concern. Consequently, measurements made at 77 K with a synchrotron radiation source generate more meaningful data and will be elaborated on in the next section.

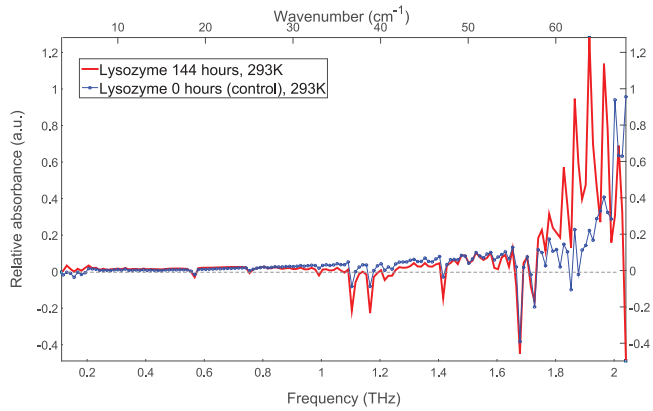

(a)

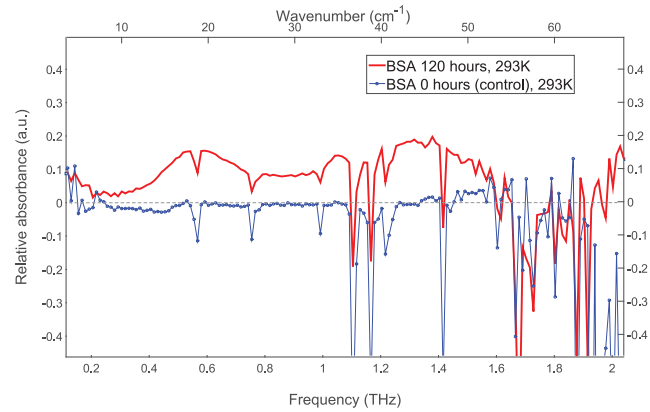

(b)

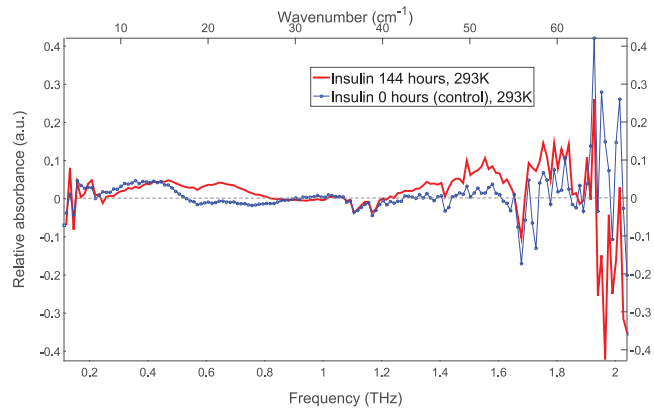

(c)

Fig. 7. THz absorbance at 293 K, obtained using a THz-TDS system. (a) Lysozyme fibrils. (b) BSA fibrils. (c) Insulin fibrils.

VI. Synchrotron Results and Discussion

As in our THz-TDS measurements, we first seek to understand how the FIR spectral profiles of aqueous native proteins held in NC differs from those of powdered proteins pressed with HDPE in a pellet. Fig. 8(a) and (b) present a comparison of all three proteins in the FIR frequency range. It is important to note here that thoroughly air-drying the aqueous samples is essential to avoid ice formation. We have found that visual inspection of dryness is sufficient to avoid this. Furthermore, indications of ice formation appears in the region between 3–10 THz (as confirmed in [31]) where the THz absorbance increases significantly.

A broad peak at $\approx$5 THz is present in all plots in Fig. 8(a) and (b). This broad peak is typical for globular proteins [32]. Furthermore, the shape of the spectral profiles are very similar in the low FIR region [33]. It is interesting to note

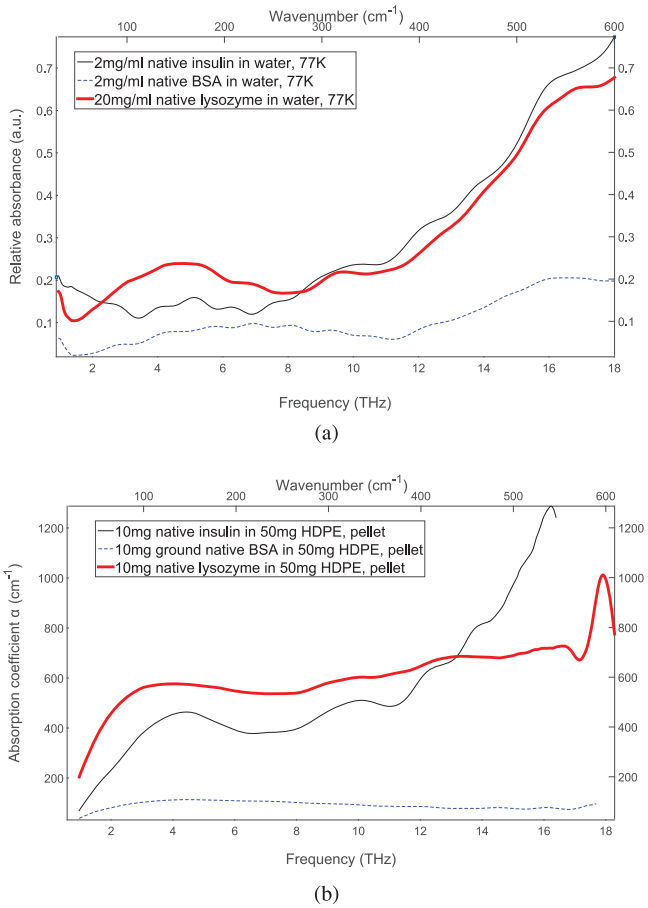

Fig. 8. THz absorbance and absorption of native proteins in the FIR range when (a) held in NC at 77 K with no ice present and (b) measured as pellets at 293 K.

that the THz absorbance and absorption coefficient of BSA are distinctly lower than those of lysozyme and insulin regardless if measured as a pellet or in NC. The similar trends between Fig. 8(a) and (b) aid in confirming that we do not lose spectral integrity from holding our aqueous samples in NC.

A. Lysozyme Fibrils

Fig. 9 presents the synchrotron results for lysozyme fibrils. The 0- and 72-h plots diverge from 5–10.5 THz and are in agreement with the observations in [11]. The new observations from this work are: 1) the 24- and 72-h plots are very similar and mostly overlap; 2) beyond 10.5 THz, the 0-, 24- and 72-h plots converge and continue to rise; and 3) there is a steep rise in the 144-h plot with a reduction in the dip at ≈10 THz.

For observations 1) and 2), cross-referencing against the 24- and 72-h TEM images reveal that there are few aggregates at 24 h whereas fibril-like clumps are present at 72 h, but these clumps have not significantly altered the THz absorbance. In [11], where the THz absorbance of 0- and 69-h-old lysozyme fibrils are analyzed up to 10.5 THz, scattering from the cylindrical fibers was proposed as the cause for the distinction between THz absorbance. Cylindrical scatterers with dimensions in the order as those found in this work (tens to hundreds of nanometers for 72-h-old fibrils) generate a $1/\lambda^4$ Rayleigh scattering profile (where λ is the wavelength), as shown by the

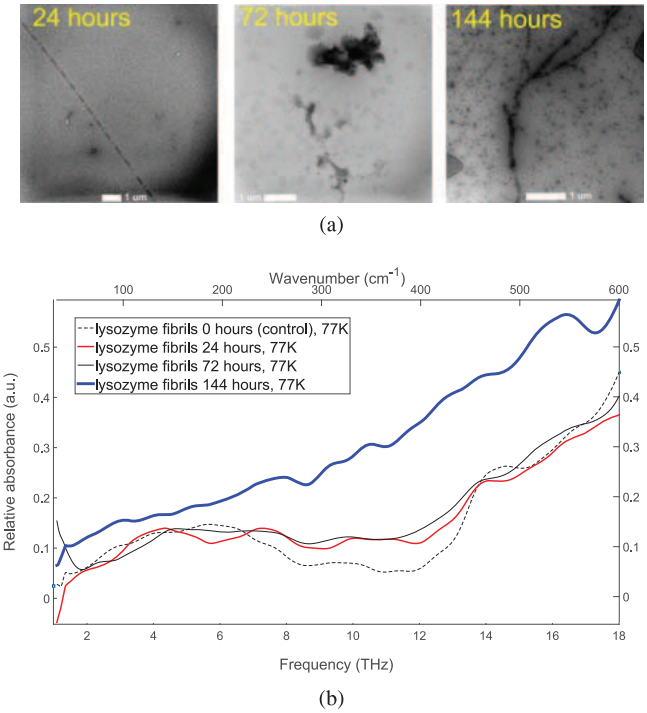

Fig. 9. (a) TEM micrographs of lysozyme fibrils; scale bar representation: 1 μm for all figures. (b) THz absorbance of lysozyme fibrils measured at 77 K using a synchrotron radiation source.

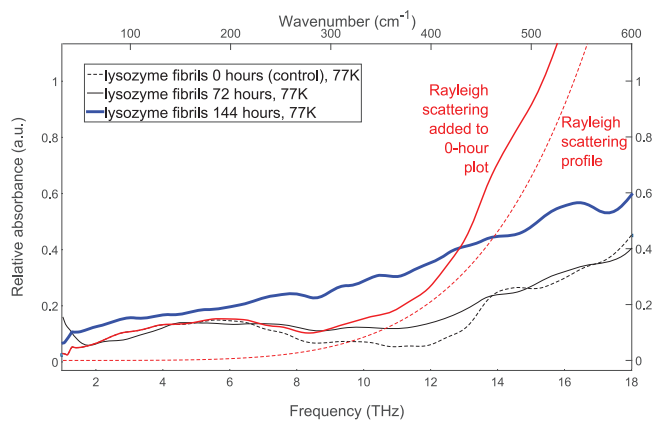

Fig. 10. Rayleigh scattering added to the 0-h plot and compared with plots from 72 and 144 h.

dotted red lines in Fig. 10. We would expect increasing distinction in the THz absorbance across the higher frequencies but we do not observe this in our work. Scattering from fibrils is therefore not likely to be the sole cause of the observed differences in THz absorbance in our work.

For observation 3), unlike the clumps, the presence of thick fibrils at 144 h does alter the THz absorbance profile. As seen in Fig. 10, scattering is again unlikely to be the sole cause of the reduction in the dip at ≈10 THz. In a study of nonheat treated and heat-treated β-lactoglobulin fibrils at pH 7, broad spectral changes occurring between 4.5–12 THz were attributed to interprotein disulfide bridges [34] because several Raman spectral lines were reported between 4.5–12 THz for lyophilized crystalline cystine (an amino acid) that contains disulfide bridges [35].

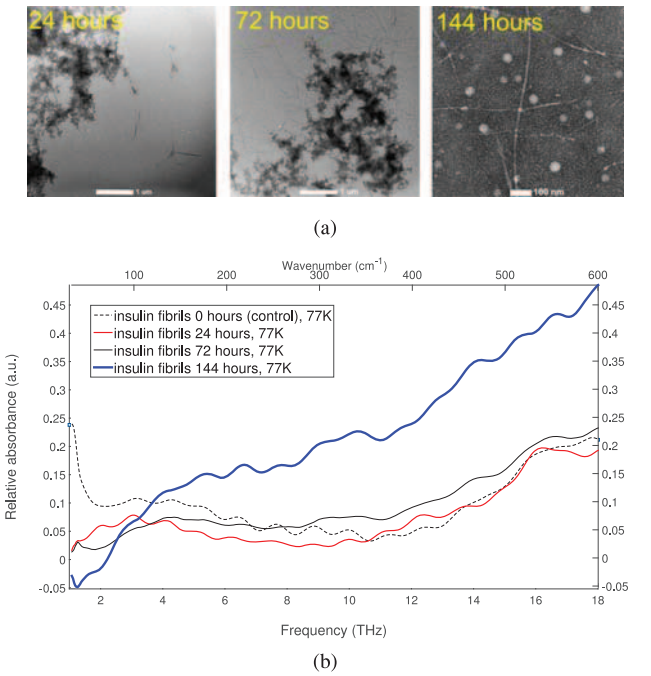

Fig. 11. (a) TEM micrographs of insulin fibrils; scale bar representation: 1 μm for 24 and 72 h and 100 nm for 144 h. (b) THz absorbance of insulin fibrils measured at 77 K using a synchrotron radiation source.

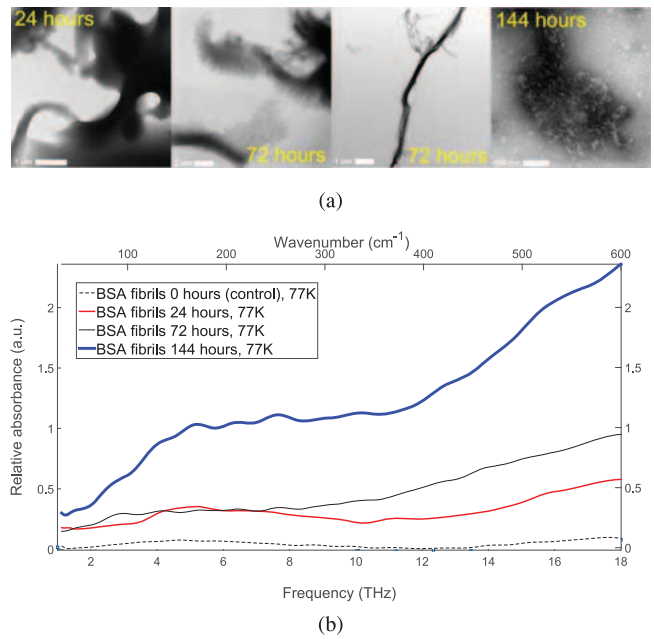

Fig. 12. (a) TEM micrographs of BSA fibrils; scale bar representation: 1 μm for 24 h, 2 μm (left) and 1 μm (right) for 72 h, and 100 nm for 144 h. (b) THz absorbance of BSA fibrils measured at 77 K using a synchrotron radiation source.

Disulfide bridges are covalent bonds between two sulfur atoms that constraint the secondary and tertiary structure of proteins, such as the shape of fibrils [36]. A disulfide bridge can be thought of as a damped spring between two partially rigid bodies (sulfur atoms) whereby the spring has limited degrees of freedom to move (e.g., in and out of plane, twisting), and that its movements generate resonant frequencies.

A native lysozyme molecule has four disulfide bridges that remain intact after formation of amyloid fibrils but these bridges become exposed to the aqueous medium [37]. Exposed disulfide bridges are also found in insulin and BSA [38], [39]. Coincidentally, the reduction in the dip at ≈10 THz is similarly observed in insulin and BSA (Sections VI-B and VI-C).

As mentioned above, there are several Raman lines in the 10-THz region that were attributed to disulfide bridges in crystalline cystine. In [40], however, the exposed disulfide bridges of BSA in an acidic solution was reported to have different atomic arrangements (conformations) from crystalline BSA. Further investigation is therefore needed to explore the differences or similarities between the exposed disulfide bridges in fibrils and those in crystalline cystine before any connections can be drawn with our observation at 10 THz.

Interestingly, the core structure of a lysozyme amyloid fibril only contains around 50% of the original native lysozyme molecule [41]. The remaining native lysozyme does not form β-sheets and is dissolved in the buffer used to synthesize the fibrils (i.e., the supernatant). The chemical composition of the lysozyme amyloid fibrils therefore differs from that of native lysozyme. This may be the reason why the THz absorbance profile of lysozyme fibrils appears more linear than those of insulin and BSA fibrils that will be presented next.

B. Insulin Fibrils

Fig. 11 presents the synchrotron results for insulin fibrils. Unlike observation 1) for lysozyme, the 24- and 72-h plots for insulin do not overlap above ≈4.5 THz. Cross-referencing against the 24- and 72-h TEM images, fine insulin fibrils are present at 72 h but not at 24 h, thus the difference between the two absorbance profiles may indeed be due to the fine fibrils. Like lysozyme, the presence of thick fibrils at 144 h significantly alters the THz absorbance profile and there is again a reduction in the dip at ≈10 THz. Similar to lysozyme, native insulin has three disulfide bridges that also remain intact after formation of amyloid fibrils [38] but, unlike lysozyme, nearly all of the native insulin molecule aggregate to become insulin fibrils [42]. The similar chemical composition of native insulin and insulin fibrils may be the reason for the similar shape in their THz absorbance profiles.

C. BSA Fibrils

Fig. 12 presents the synchrotron results for BSA fibrils. As seen from the TEM images, aggregation occurs rapidly in BSA with clumps forming within 24 h. At 72 h, both thick fibrils and clumps. Interestingly by 144 h, the thick fibrils aggregate further into a dense network of curly fibrils as reported in [21]. These curly fibrils are unlike the straight, needle-like fibrils formed in lysozyme and insulin.

There is a very distinct difference between the 24- and 72-h THz absorbance profiles of BSA unlike those observed in lysozyme and insulin. The 72-h profile has a reduced dip at ≈10 THz and rises upward like the 144-h THz absorbance plots for thick lysozyme and insulin fibrils. This may possibly be due to the additional presence of thick BSA fibrils at 72 h when compared to 24 h. Like lysozyme and insulin, native BSA

contains 17 disulfide bridges that remain intact after formation of amyloid fibrils [39].

At 144 h, the dip at ≈10 THz is observed again, but the absorbance magnitude is significantly higher than at 72 h. In [21], X-ray diffraction results revealed that BSA fibrils contain a mix of morphologies rather than a one single type of β-pleated structure as found in lysozyme and insulin fibrils. The initial reduction and subsequent return of the dip at 10 THz suggest contribution from several subtypes of aggregates not found in lysozyme and insulin fibrils at 144 h [21]. These subtypes of aggregates appear to produce a similar broad peak that we observed in native BSA and BSA fibrils at 0 and 24 h.

It is interesting to note that both ThT fluorescence and CD assays have confirmed the presence of β-sheets and fibrils at 144 h but they could not reveal any additional information about the secondary structure of BSA. Far-infrared spectroscopy however appears to be able to reveal the transition from globular protein to classical needle-like fibrils to curly ropes of fibrils. This would be advantageous to quality control applications (e.g., controlling aggregation in dairy products) whereby the aggregation process can be monitored without the need for lyophilization.

VII. Conclusion

This work has utilized THz and FIR spectroscopies to track the fibrillation of lysozyme, insulin and BSA fibrils that have been incubated up to 144 h. The room temperature THz-TDS results do not shed light on the intrinsic nature of the fibrils due to residual water in the samples. While this outcome is not useful in this particular work, it is potentially useful for studying water activity in close proximity to the fibrils.

The FIR results indicate that thick, straight mature fibrils from all three proteins distinctly absorb more FIR radiation than their intermediate aggregates, which can be an indicator for tracking aggregation. Scattering is unlikely the sole cause of the strong absorbance as there is a reduction of a dip at 10 THz that cannot be explained using scattering theory. This reduction at 10 THz may be a characteristic of mature fibrils but further investigation is needed to ascertain this together with the influence of disulfide bridges on the measured signal. The unusual aggregation of BSA into curly fibrils is not revealed by fluorescence and CD assays but appears to be captured by FIR spectroscopy. An open question for future work is to include the use of FIR spectroscopy to explore the effects of twists in fibrils.

Acknowledgment

The authors would like to thank D. Appadoo, R. Plathe, S. Zhu, and D. Valchev for their assistance at the Australian Synchrotron. This work was performed at the University of Adelaide and the Australian Synchrotron; TEM work was performed at Adelaide Microscopy; CD work was performed at the University of South Australia.

References

[1] W. Wang, "Protein aggregation and its inhibition in biopharmaceutics," *Int. J. Pharmaceutics*, vol. 289, no. 1–2, pp. 1–30, 2005.

[2] A. Fink, "Protein aggregation: Folding aggregates, inclusion bodies and amyloid," *Folding and Design*, vol. 3, no. 1, pp. R9–R23, 1998.

[3] M. Krebs, G. Devlin, and A. Donald, "Protein particulates: Another generic form of protein aggregation?," *Biophys. J.*, vol. 92, no. 4, pp. 1336–1342, 2007.

[4] U. Shimanovich, I. Efimov, T. Mason, P. Flagmeier, A. Buell, A. Gedanken, S. Linse, K. Åkerfeldt, C. Dobson, D. Weitz, and T. Knowles, "Protein microgels from amyloid fibril networks," *ACS Nano*, vol. 9, no. 1, pp. 43–51, 2015.

[5] Y.-H. Zhang and L.-H. Huang, "Effect of heat-induced formation of rice bran protein fibrils on morphological structure and physicochemical properties in solutions and gels," *Food Sci. Biotechnol.*, vol. 23, no. 5, pp. 1417–1423, 2014.

[6] M. Hineno and H. Yoshinaga, "Far-infrared spectra of galactose and lactose at liquid He temperature," *Spectr. Acta A, Molecular Biomolecular Spectroscopy*, vol. A29, no. 2, pp. 301–305, 1973.

[7] M. Hineno and H. Yoshinaga, "Far-infrared spectra of β-D-glucose, cellobiose, galactose, lactose, α-D-glucose and saccharose in 50–30 cm^{-1} at liquid He temperature," *Spectr. Acta A, Molecular Biomolecular Spectroscopy*, vol. A29, no. 8, pp. 1575–1578, 1973.

[8] P. Upadhya, Y. Shen, A. Davies, and E. Linfield, "Far-infrared vibrational modes of polycrystalline saccharides," *Vibrational Spectroscopy*, vol. 35, no. 1–2, pp. 139–143, 2004.

[9] M. Ataka and S. Tanaka, "Far-infrared spectrum of crystalline lysozyme," *Biopolymers*, vol. 18, no. 3, pp. 507–516, 1979.

[10] G. Acbas, K. Niessen, E. Snell, and A. Markelz, "Optical measurements of long-range protein vibrations," *Nature Commun.*, vol. 5, p. 3076, 2014.

[11] H. Zakaria, B. Fischer, A. Bradley, I. Jones, D. Abbott, A. Middelberg, and R. Falconer, "Low-frequency spectroscopic analysis of monomeric and fibrillar lysozyme," *Appl. Spectroscopy*, vol. 65, no. 3, pp. 260–264, 2011.

[12] R. Liu, M. He, R. Su, Y. Yu, W. Qi, and Z. He, "Insulin amyloid fibrillation studied by terahertz spectroscopy and other biophysical methods," *Biochem. Biophys. Res. Commun.*, vol. 391, no. 1, pp. 862–867, 2010.

[13] M. Stefani and C. Dobson, "Protein aggregation and aggregate toxicity: New insights into protein folding, misfolding diseases and biological evolution," *J. Molecular Medicine*, vol. 81, no. 11, pp. 678–699, 2003.

[14] A. Jan, D. Hartley, and H. Lashuel, "Preparation and characterization of toxic Aβ aggregates for structural and functional studies in Alzheimer's disease research," *Nature Protocols*, vol. 5, no. 6, pp. 1186–1209, 2010.

[15] H. Hampel, Y. Shen, D. Walsh, P. Aisen, L. Shaw, H. Zetterberg, J. Trojanowski, and K. Blennow, "Biological markers of amyloid beta-related mechanisms in Alzheimer's disease," *Experimental Neurol.*, vol. 223, no. 2, pp. 334–346, 2010.

[16] E. Foegeding and J. Davis, "Food protein functionality: A comprehensive approach," *Food Hydrocolloids*, vol. 25, no. 8, pp. 1853–1864, 2011.

[17] R. Mezzenga and P. Fischer, "The self-assembly, aggregation and phase transitions of food protein systems in one, two and three dimensions," *Rep. Progress in Phys.*, vol. 76, no. 4, 2013, Art. ID 046601.

[18] T. McCann, A. Leder, R. Buckow, and L. Day, "Modification of structure and mixing properties of wheat flour through high-pressure processing," *Food Res. Int.*, vol. 53, no. 1, pp. 352–361, 2013.

[19] H.-C. Mahler, W. Friess, U. Grauschopf, and S. Kiese, "Protein aggregation: Pathways, induction factors and analysis," *J. Pharmaceutical Sci.*, vol. 98, no. 9, pp. 2909–2934, 2009.

[20] F. Chiti and C. Dobson, "Amyloid formation by globular proteins under native conditions," *Nature Chemical Biol.*, vol. 5, no. 1, pp. 15–22, 2009.

[21] N. Holm, S. Jespersen, L. Thomassen, T. Wolff, P. Sehgal, L. Thomsen, G. Christiansen, C. Andersen, A. Knudsen, and D. Otzen, "Aggregation and fibrillation of bovine serum albumin," *Biochimica Et Biophysica Acta-Proteins and Proteomics*, vol. 1774, no. 9, pp. 1128–1138, 2007.

[22] K. Bruggink, M. Müller, H. Kuiperij, and M. Verbeek, "Methods for analysis of amyloid-β aggregates," *J. Alzheimer's Disease*, vol. 28, no. 4, pp. 735–758, 2012.

[23] S. Kelly, T. Jess, and N. Price, "How to study proteins by circular dichroism," *Biochimica Biophysica Acta*, vol. 1751, no. 2, pp. 119–139, 2005.

[24] R. Khurana, C. Coleman, C. Ionescu-Zanetti, S. Carter, V. Krishna, R. Grover, R. Roy, and S. Singh, "Mechanism of thioflavin T binding to amyloid fibrils," *J. Structural Biol.*, vol. 151, no. 3, pp. 229–238, 2005.

[25] G. Png, R. Falconer, B. Fischer, H. Zakaria, S. Mickan, A. Middelberg, and D. Abbott, "Terahertz spectroscopic differentiation of microstructures in protein gels," *Opt. Exp.*, vol. 17, no. 15, pp. 13 102–13 115, 2009.

[26] G. Png, B. Fischer, D. Appadoo, R. Plathe, and D. Abbott, "Double-layered nitrocellulose membrane sample holding technique for THz and FIR spectroscopic measurements," *Opt. Exp.*, vol. 23, no. 4, pp. 4997–5013, 2015.
[27] M. van Exter, C. Fattinger, and D. Grischkowsky, "Terahertz time-domain spectroscopy of water vapor," *Opt. Lett.*, vol. 14, no. 20, pp. 1128–1130, 1989.
[28] X. Xin, H. Altan, A. Saint, D. Matten, and R. Alfano, "Terahertz absorption spectrum of *para* and *ortho* water vapors at different humidities at room temperature," *J. Appl. Phys.*, vol. 100, no. 9, 2006, Art. ID 094905.
[29] A. McIntosh, B. Yang, S. Goldup, M. Watkinson, and R. Donnan, "Crystallization of amorphous lactose at high humidity studied by terahertz time domain spectroscopy," *Chem. Phys. Lett.*, vol. 558, pp. 104–108, 2013.
[30] W. Wang, "Lyophilization and development of solid protein pharmaceuticals," *Int. J. Pharmaceutics*, vol. 203, no. 1–2, pp. 1–60, 2000.
[31] G. Profeta and S. Scandolo, "Far-infrared spectrum of ice Ih: A first-principles study," *Phys. Rev. B*, vol. 84, no. 2, 2011, Art. ID 024103.
[32] U. Buontempo, G. Careri, P. Fasella, and A. Ferraro, "Far-infrared spectra of some globular proteins," *Biopolymers*, vol. 10, no. 12, pp. 2377–2386, 1971.
[33] A. Mott and P. Rez, "Calculation of the infrared spectra of proteins," *Eur. Biophys. J. Biophys. Lett.*, vol. 44, no. 3, pp. 103–112, 2015.
[34] R. Falconer, H. Zakaria, Y. Fan, A. Bradley, and A. Middelberg, "Far-infrared spectroscopy of protein higher-order structures," *Appl. Spectroscopy*, vol. 64, no. 11, pp. 1259–1264, 2010.
[35] N. Brandt, A. Chikishev, A. Kargovsky, M. Nazarov, O. Parashchuk, D. Sapozhnikov, I. Smirnova, A. Shkurinov, and N. Sumbatyan, "Terahertz time-domain and Raman spectroscopy of the sulfur-containing peptide dimers: Low-frequency markers of disulfide bridges," *Vibrational Spectroscopy*, vol. 47, no. 1, pp. 53–58, 2008.
[36] J. Jiménez, E. Nettleton, M. Bouchard, C. Robinson, C. Dobson, and H. Saibil, "The protofilament structure of insulin amyloid fibrils," in *Proc. Nat. Acad. Sci.*, 2002, vol. 99, no. 14, pp. 9196–9201.
[37] M. Dumoulin, J. Kumita, and C. Dobson, "Normal and aberrant biological self-assembly: Insights from studies of human lysozyme and its amyloidogenic variants," *Accounts of Chem. Res.*, vol. 39, no. 9, pp. 603–610, 2006.
[38] D. Kurouski, J. Washington, M. Ozbil, R. Prabhakar, A. Shekhtman, and I. Lednev, "Disulfide bridges remain intact while native insulin converts into amyloid fibrils," *PLOSONE*, vol. 7, no. 6, 2012, Art. ID e36989.
[39] M. Yang, C. Dutta, and A. Tiwari, "Disulfide-bond scrambling promotes amorphous aggregates in lysozyme and bovine serum albumin," *J. Phys. Chem. B*, vol. 119, no. 10, pp. 3969–3981, 2015.
[40] K. Nakamura, S. Era, Y. Ozaki, M. Sogami, T. Hayashi, and M. Murakami, "Conformational changes in seventeen cystine disulfide bridges of bovine serum albumin proved by Raman spectroscopy," *FEBS Lett.*, vol. 417, no. 3, pp. 375–378, 1997.
[41] E. Frare, M. Mossuto, P. de Laureto, M. Dumoulin, C. Dobson, and A. Fontana, "Identification of the core structure of lysozyme amyloid fibrils by proteolysis," *J. Molecular Biol.*, vol. 361, no. 3, pp. 551–561, 2006.
[42] E. Chatani, H. Imamura, N. Yamamoto, and M. Kato, "Stepwise organization of the beta- structure identifies key regions essential for the propagation and cytotoxicity of insulin amyloid fibrils," *J. Biological Chemistry*, vol. 289, no. 15, pp. 10 399–10 410, 2014.

Gretel M. Png (M'98) received the B.Eng. degree (with first class Honors) in electrical and electronics engineering from the University of Edinburgh, Edinburgh, U.K., in 1997, the M.Sc. degree in electrical engineering and computer science from the University of California, Irvine, CA, USA, in 2004, and the Ph.D. degree (with a Dean's commendation) in electrical and electronics engineering from the University of Adelaide, Adelaide, Australia, in 2010 under Brian Ng, Derek Abbott, and Sam Mickan in the area of terahertz spectroscopy and modeling of biotissue.

She is currently an Australian Research Council Discovery Early Career Researcher Award (DECRA) Postdoctoral Research Fellow. Her current research focuses on terahertz, far-infrared, and mid-infrared spectroscopies of fibrillar proteins. She has worked as a Radar Systems Engineer and an Electrical Design Engineer from 1997 to 2001 in Sweden, Israel, and Singapore. Her other research interests are in scattering theory, bioelectromagnetics, molecular dynamics, STEM teaching in schools, e-learning, and *edutainment* for learning.

Dr. Png won the Harold Dickinson Memorial Prize at the University of Edinburgh, the University of California at Irvine Excellence in Teaching Award, the prestigious Australian Postgraduate Award (APA) scholarship, the SPIE Educational Scholarship in Optical Science and Engineering (2006, 2007), and several University of Adelaide administered undergraduate awards and postdoctoral grants (Research Abroad Scholarship 2005, Mutual Community Postgraduate Travel Grant 2005, AUGU/RC Heddle Award 2006, Faculty Research Support Grant 2014 and 2015). She was the Faculty of Engineering, Computer and Mathematical Science's winner and representative at the University of Adelaide's inaugural 3-Minute Thesis competition in 2010. She was Chair of the IEEE Student Branch at the University of Adelaide in 2006/2007 and was actively involved in undergraduate teaching.

Robert J. Falconer received the B.Sc. degree in biotechnology from the University of New South Wales, Australia, in 1983, and the Ph.D. degree in chemical engineering from the University of Adelaide, Adelaide, Australia, in 1997.

He was a Research Scientist with Biotech Australia Pty Ltd (1984–1992), Sydney, Australia, and then a Production Scientist with GroPep Pty Ltd (1992–1995), Adelaide, Australia. Following a period as a Production Manager with Tuta Healthcare Pty Ltd (2000–2002), he became a Bioscience Research Coordinator with the University of Cambridge, Cambridge, U.K. (2003–2006). He then took up an appointment as a Research Fellow at the University of Queensland, Australia (2007–2011), and since 2011 has been a Senior Lecturer with the University of Sheffield, Sheffield, U.K. His research is focused on the application of terahertz spectroscopy and micro-calorimetry to understand the interaction between proteins, water, and small molecules.

Derek Abbott (M'85–SM'99–F'05) was born in London, U.K., in 1960. He received the B.Sc. (Hons.) degree in physics from Loughborough University, Loughborough, U.K., in 1982, and the Ph.D. degree in electrical and electronic engineering from the University of Adelaide, Adelaide, Australia, in 1995, under K. Eshraghian and B. R. Davis.

From 1978 to 1986, he was a Research Engineer with the GEC Hirst Research Centre, London, U.K. From 1986 to 1987, he was a VLSI Design Engineer with Austek Microsystems, Australia. Since 1987, he has been with the University of Adelaide, where he is presently a Full Professor with the School of Electrical and Electronic Engineering. He holds over 800 publications/patents and has been an invited speaker at over 100 institutions. He has served as an editor and/or guest editor for a number of journals, including *Journal of Optics B*, *Microelectronics Journal*, and *PLOSONE*. He is currently on the editorial boards of Nature's *Scientific Reports* and *Royal Society Online Science*. He coedited *Quantum Aspects of Life* (Imperial College, 2008), coauthored *Stochastic Resonance* (Cambridge University, 2008), and coauthored *Terahertz Imaging for Biomedical Applications* (Springer-Verlag, 2012). His research interest is in the area of multidisciplinary physics and electronic engineering applied to complex systems. His research programs span a number of areas of stochastics, game theory, photonics, biomedical engineering, and computational neuroscience.

Prof. Abbott is a Fellow of the Institute of Physics (IOP). He has won a number of awards including the South Australian Tall Poppy Award for Science (2004), the Premier's SA Great Award in Science and Technology for outstanding contributions to South Australia (2004), and an Australian Research Council (ARC) Future Fellowship (2012). He has served as an editor and/or guest editor for a number of journals, including the IEEE JOURNAL OF SOLID-STATE CIRCUITS, the PROCEEDINGS OF THE IEEE, and the IEEE PHOTONICS JOURNAL. He is currently on the editorial board of IEEE ACCESS.